

Super Bending-Stable Flexible Colloidal QD Photodetector with Fast Response and Near-Unity Carrier Extraction Efficiency

Yu-Hao Deng,* Ezat Kheradmand, Chao Pang, Abu Bakar Siddik, Jing Bai, Itai Lieberman, Pieter Geiregat, Dries Van Thourhout, and Zeger Hens*



Cite This: *ACS Appl. Mater. Interfaces* 2025, 17, 14243–14249



Read Online

ACCESS |

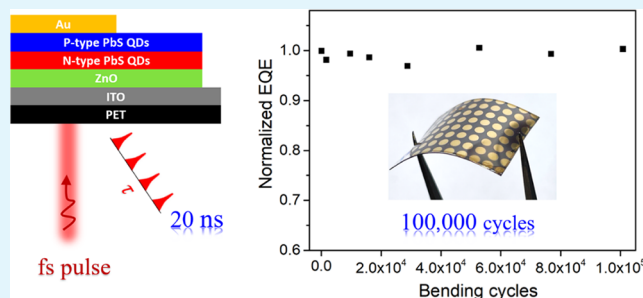
Metrics & More

Article Recommendations

Supporting Information

ABSTRACT: Flexible colloidal quantum dot (QD) optoelectronics apply the superior properties of colloidal QDs to flexible devices, exhibiting unique advantages in the fields of imagers, solar cells, displays, wearable sensors, on-skin electronics, robotics, and bioimaging. Here, we show that colloidal QD photodiodes (QDPDs) with an ultrathin QD absorber layer have record bending stability with 100,000 repetitive bending cycles in QD devices. The QDPDs obtained a high-quality p–n junction with a 1700 rectification ratio. The formation of a Fabry–Pérot cavity by the layered stack results in a 3.4-fold enhanced light absorption, while the ultrathin structure ensures a near-unity efficient extraction (97%) of photogenerated charge carriers from the PbS QD film upon illumination with 1330 nm short-wavelength infrared light. Finally, upon suppression of the capacitance effect, the response time of this QDPD can be as short as 20 ns, which is the fastest response for flexible colloidal QDPDs.

KEYWORDS: flexible optoelectronics, bending stability, colloidal quantum dots, photodetector, short-wave infrared



INTRODUCTION

Thin-film devices based on colloidal quantum dots (QDs) show unique advantages for flexible optoelectronics, with applications ranging from flexible imagers, solar cells, or displays to wearable sensors, on-skin electronics, robotics, and bioimaging.^{1–3} In particular, QD-based devices hold the promise of being bendable, lightweight, and processable across multiple length scales, which are all required features for flexible optoelectronics.^{4–8} Moreover, as an optoelectronic material, QDs feature easily tunable properties and are suitable for cost-effective solution-based processing.^{2,9–15} Flexible QD-based devices, however, often suffer from failure, as repeated bending compromises the device integrity and deteriorates performance. Bending strain, for example, is known to induce cracks in thin films, which lead to the degradation of flexible structures.^{16,17} Stress relaxation in strained films can lead to crack formation/propagation,¹⁸ or interfacial delamination. Obviously, such changes in the device structure limit the durability of flexible QD optoelectronic devices,^{19,20} especially when proper operation depends on charge transport through a QD film or charge transfer at interfaces.^{18,21} With growing demands for reliable flexible optoelectronics with stable performance therefore comes the requirement for bending stability of the components.

Considerable progress has been made in overcoming issues with the bending stability for flexible colloidal QD optoelectronics. Adaptations such as enhancing interface adhesion²²

and introducing polyimide to improve QD passivation and film morphology have been proposed to improve the bending stability,²³ while flexible electrodes,^{24,25} electron transporting layers (ETL),^{26,27} and active layers^{28–31} have been introduced to improve the mechanical properties of thin-film devices. Quantitatively, the best-reported QD photodetector maintained 88% of the initial photocurrent after 12,000 bending cycles,³² a result that still needs further improvement in view of the increasing demand of applications that require high bending stability, such as portable flexible solar cells, displays and imagers, wearable sensors for sports and medical use. Interestingly, a number of studies indicate that thinner films may suffer less from bending-induced damage.^{33–35} Supported 100 nm-thick Cu films, for example, were found to withstand 100 times as many bending cycles than similarly strained, 3.75 μm-thick films,³³ while photodetectors using 20 nm thin perovskite films did not show damage after 1000 bending cycles, in contrast to similar devices with 200 or 600 nm-thick film.³⁵ Such results suggest that reducing the film thickness

Received: December 16, 2024

Revised: January 30, 2025

Accepted: February 7, 2025

Published: February 19, 2025



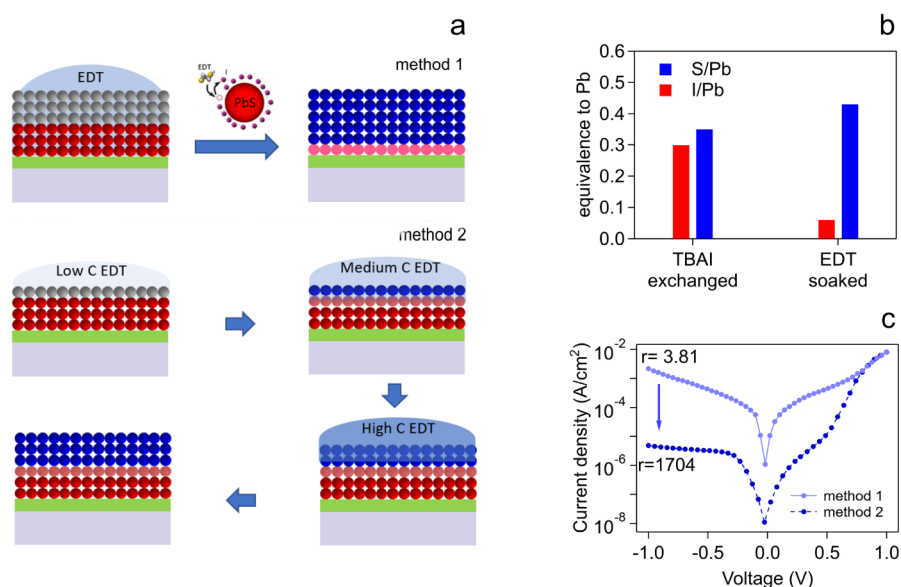


Figure 1. (a) Depiction of the different methods used to fabricate a stack of ultrathin n-PbS and p-PbS QDs, indicating in method 1 the traditional method and in method 2 the concentration gradient ligand exchanged method. The gray balls mean the colloidal QDs before ligand exchange, the red balls mean n-type QD ligands exchanged by TBAI, and the blue balls mean p-type QD ligands exchanged by EDT. (b) Element analysis of I/Pb and S/Pb molar ratio of TBAI-exchanged film and TBAI-exchanged film after soaking in the EDT solution as measured by X-ray fluorescence (XRF) spectroscopy. (c) Dark current measured with -1 to $+1$ V applied voltage of the QDPDs consisting of 50 nm n-type and 50 nm p-type QD films, fabricated via methods 1 and 2.

could also improve bending stability for devices based on thin QD films.

Here, we demonstrate ultrathin PbS QD photodiodes (QDPDs) that offer record bending stability while remaining efficient detectors of infrared light. We combined these characteristics by counteracting the reduced absorption in a thin QD film through the formation of a Fabry–Pérot cavity in the QDPD stack that enhances light absorption by 3.4-fold. The ultrathin devices have a 50 nm-thick active layer, in which we implement a p–n junction by gradually shifting the QD surface treatment from yielding n-type to yielding p-type PbS QD films, an approach that avoided any in situ change in doping type during film formation. The resulting QDPDs have a pronounced $+1/-1$ V rectification ratio of 1700, a carrier-extraction efficiency of 97%, and a record response time of 20 ns. The idea that thinner films suffer less from bending-induced damage is confirmed by experimental observations showing crack formation in QDPDs with thicker QD films but not in thinner films. In line with this observation, such QDPDs show no signs of breakdown after 100,000 repetitive bending cycles. These results indicate that designing QDPDs with an ultrathin active layer is a viable path toward realizing the combination of super bending stability and high performance for flexible colloidal QD photodetectors.

RESULTS AND DISCUSSION

In this work, we fabricated QDPDs with thin absorber layers by sandwiching a film of n-type PbS QDs with a band gap absorption at 1330 nm between n-ZnO and a film of p-type PbS QDs with a band gap absorption at 950 nm. Details on the QD synthesis and an overview of QD characteristics can be found in Supporting Information S1. As outlined in Supporting Information S2, we fabricated QDPDs using these QDs by means of repetitive spin coating and solid-state ligand exchange. First, a flexible substrate (PET/ITO) was stuck on a glass support with a double-sided tape, after which we formed

an electron transfer layer (ETL) by spin coating a layer of ZnO nanocrystals on the ITO-coated PET. Next, we spun a film of oleate-capped QDs and extracted the oleate ligands by dropping a solution of tetrabutylammonium iodide (TBAI) on top of the QD film, a known procedure to form an n-PbS QD film.³⁶ An additional layer of p-PbS QDs was formed in a similar way using a solution of ethanedithiol (EDT) for extracting the oleate ligands.³⁶

In line with a previous work,¹³ we first integrated ultrathin diode stacks through the sequential deposition of a 50 nm n-type and a 50 nm p-type PbS QD layer in a flexible system, as schematically depicted in Figure 1a (method 1 on the flexible PET/ITO/ZnO substrate). However, the resulting stacks exhibited a substantial dark current of 2.18 mA/cm² at -1 V reverse bias and a rectification ratio of only 3.81 at $+1/-1$ V bias. In agreement with recent literature on QDPDs with ultrathin absorber layers,^{13,37} elemental analysis throughout the stack formation indicated that the EDT exposure reduced the amount of iodide in the PbS film (see Figure 1b). This outcome indicates that the abrupt transition from TBAI to EDT prevents the formation of a p–n junction in the PbS QD film, which probably accounts for the inferior current/voltage characteristics. To preserve the integrity of the p–n junction in the PbS QD film, we reduced the thickness of each deposited PbS QD film while gradually increasing the concentration of the EDT bath during the transition from TBAI to EDT exposure (see Figure 1a, method 2).

Supporting Information S3 provides results from field-effect (FET) transistor and UV photoelectron spectroscopy (UPS) measurements on a PbS QD film subjected to TBAI ligand exchange before and after soaking with EDT. As can be seen, TBAI treatment results in an n-PbS QD film with relatively deep CB and VB band edges and a Fermi level close to the CB edge. Moreover, EDT soaking turns this n-PbS QD film into a p-PbS film, as attested by the different FET characteristics and the upward shift of the energy levels by 0.5 eV. A similar

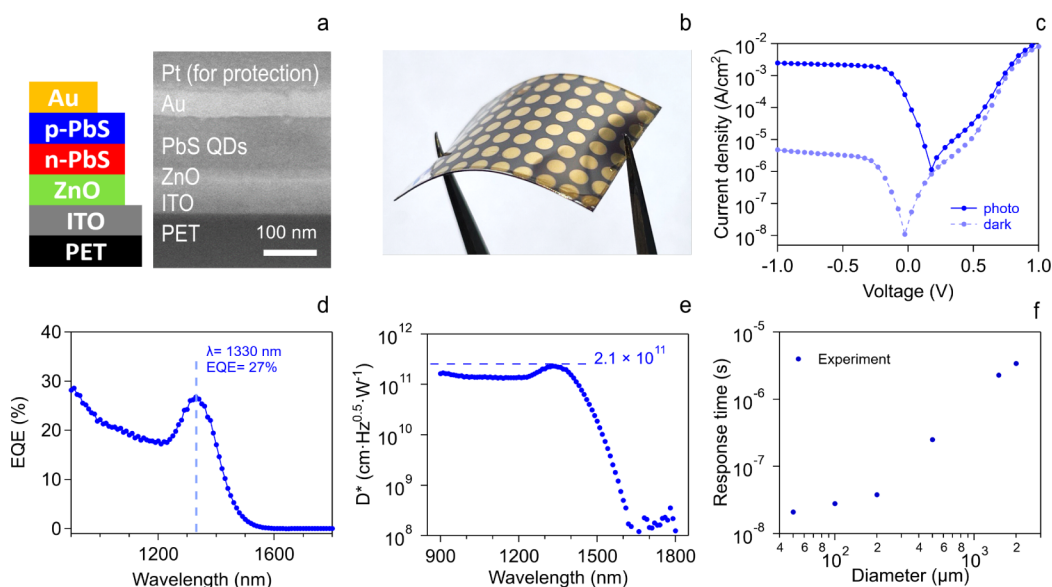


Figure 2. (a) Diagram and SEM image outlining the cross-section structure of the QDPD stack. (b) Optical photograph of the device under bending conditions, where the contact pads have a diameter of 1.5 mm. (c) J - V curve in the dark and under illumination with a 1050 nm LED. (d) Wavelength-dependent EQE of the QDPD stack, highlighting the maximum value recorded at 1330 nm. (e) Wavelength-dependent detectivity at -1 V bias. (f) Response time measurement with a variable contact pad diameter after illumination by a 100 fs, 1030 nm laser pulse.

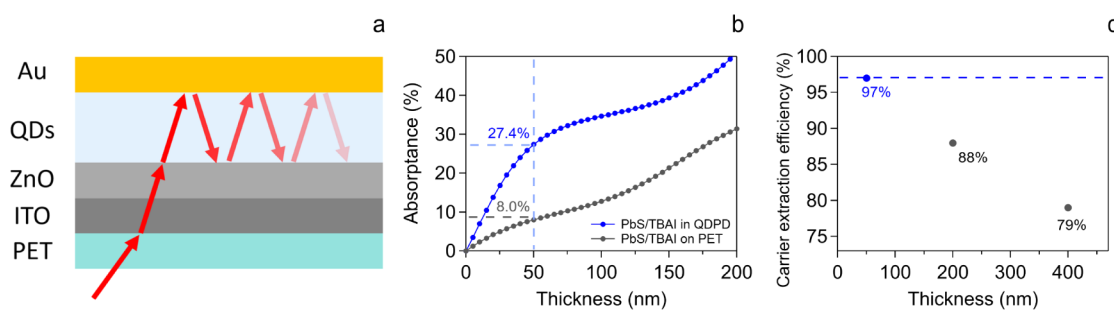


Figure 3. Absorbance enhancement and carrier extraction efficiency in photodetectors. (a) Schematic diagram of the Fabry-Pérot cavity formed by the layered stack of a QDPD. (b) Simulation of the absorbance at the exciton peak (1330 nm) as a function of the PbS layer thicknesses, either within a QDPD or on PET. As can be seen, a 50 nm-thick film exhibits a 3.4-fold enhanced absorbance. (c) Variation of the carrier extraction efficiency as a function of the active layer thickness.

exposure to a lower concentration EDT solution, however, only leads to a 0.1 eV shift of the band edges and mostly preserves the n-type character of the initial film. This surface change is gradual and concentration-dependent based on the dark current with different concentrations of EDT measured in Supporting Information S4. As demonstrated in Figure 1c, our approach significantly enhanced the performance characteristics of the QDPD on the PET substrate, probably because the densification of the PbS QDs suppresses the leaching of iodide upon transitioning to more concentrated EDT baths. Following the deposition of a gold top contact, this flexible QDPD exhibited a dark current of $4.84 \mu\text{A}/\text{cm}^2$ at -1 V reverse bias and a $+1/-1$ V rectification ratio of 1704.

Figure 2a provides a schematic representation of the QDPD stacks fabricated by using this gradual junction-formation method, where the resulting PbS QD film is sandwiched between a PET/ITO/ZnO electrode serving as the n-type contact and a gold electrode acting as the p-type contact. Elaborate details regarding the fabrication process are provided in the Methods section. The scanning electron microscopy (SEM) cross-section of a representative device stack displayed in Figure 2a confirms that this approach yields the intended

stack where the total n-PbS/p-PbS QD film has a thickness of 100 nm. Additionally, an optical photograph of the devices with a 1.5 mm diameter under bending conditions is depicted in Figure 2b. Figure 2c illustrates the current-voltage characteristics of a QDPD featuring a 50 nm-thick photoactive layer—as determined by the n-type layer of PbS QDs—in the dark and illuminated with 1030 nm light having a power density of $14.3 \text{ mW}/\text{cm}^2$. Notably, the dark current density of the ultrathin device is as low as $10^{-6} \text{ A}/\text{cm}^2$, while the photocurrent is nearly voltage-independent at -1 V bias. Moreover, as shown in Figure 2d, scanning the excitation wavelength yields a maximum external quantum efficiency (EQE) of 27% at approximately 1330 nm, a wavelength corresponding to the band gap transition of the n-PbS QDs. From noise current measurements, we calculated a maximum detectivity (D^*) of $2.1 \times 10^{11} \text{ cm Hz}^{0.5} \text{ W}^{-1}$ at 1330 nm (see Figures 2e and Supporting Information S5 for further details). Finally, Figure 2f presents the response time—defined as the time needed for the photocurrent to drop from 90 to 10% of the initial level—of a series of QDPDs that have contact pads of different diameters, upon illumination with a 100 fs laser pulse at a bias voltage of 0 V. The corresponding current

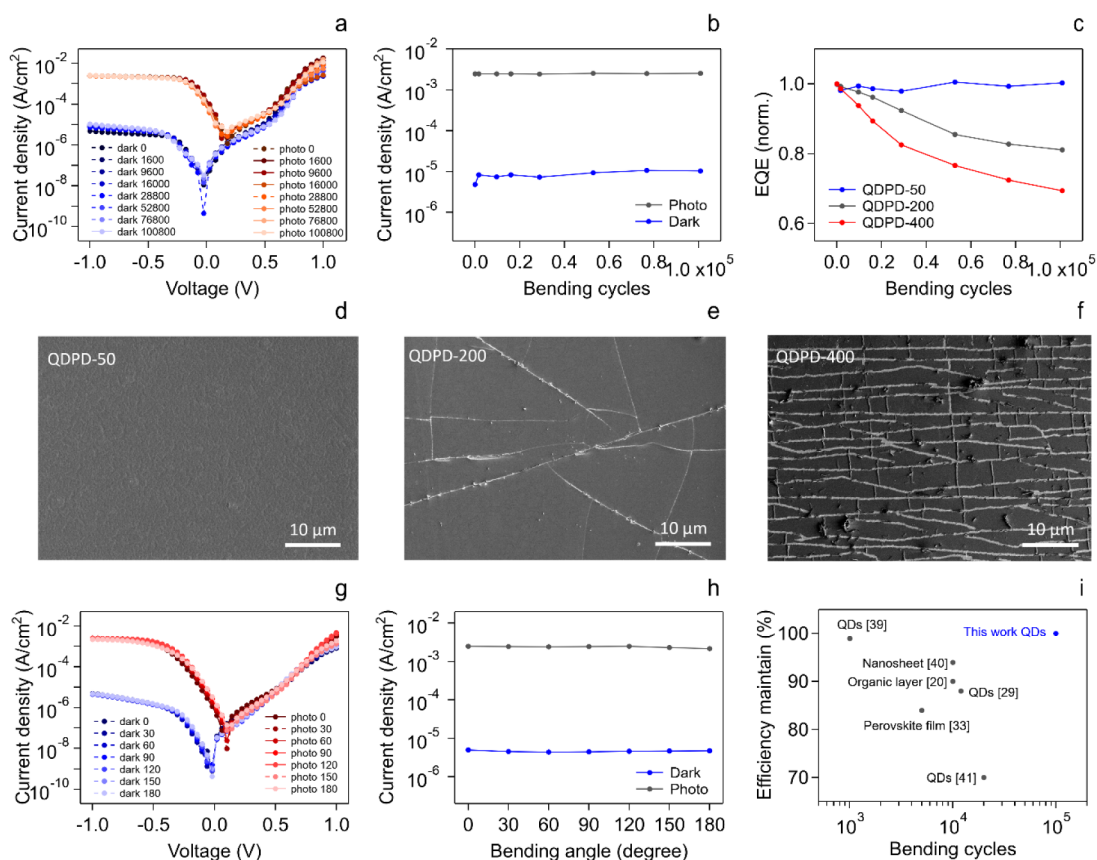


Figure 4. Bending stability of ultrathin devices. (a) J - V curves and (b) dark current and photocurrent density at -1 V of the flexible photodetector at different bending cycles. (c) EQE of QDPDs with 50, 200, and 400 nm-thick active layers on PET substrates as a function of the number of bending cycles for a bending radius of 7 mm. (d–f) SEM images of the different QDPDs as indicated after 100,000 bending cycles. With increasing film thickness, more cracks appear. (g) J - V curves and (h) dark current and photocurrent density at -1 V of the QDPD-50 at different bending angles. (i) Diagram comparing the flexible optoelectronic devices reported in this work with state-of-the-art devices in terms of remaining (relative) EQE after a given number of bending cycles.

transients are provided in Supporting Information S6. Interestingly, upon reducing the contact pad diameter to 50 μm to suppress the capacitance effect, a response time of only 20 ns is obtained, which is the shortest reported for flexible colloidal QD photodetectors.^{1,38,39}

As a rule of thumb, thinner absorber layers absorb less light, thereby reducing the quantum efficiency and detectivity of QDPDs using ultrathin absorber layers. Constructing meta-structures or plasmonic resonances can enhance light absorption by a QD film in a tunable spectral range.^{40,41} Such approaches may, however, negatively impact the integration of the active and transport layers while also adding complexity and cost to the fabrication process. As illustrated in Figure 3a, the QDPDs presented in this study address this issue through the formation of a Fabry–Pérot cavity within the QDPD stack. As outlined in Supporting Information S7, the interference within the layered QDPD stack between incident light and light reflected by the gold surface can enhance the optical field in parts of the QDPD stack, most notably the n-PbS photoactive film, which enhances the light absorption by the device. Based on optical simulations, we estimate that the light absorption by a 50 nm QD layer at 1330 nm can increase in this way from 8.0% for a film on ITO/PET to 27.4% for the same film within the QDPD, i.e., a 3.4-fold enhancement (see Figure 3b). We confirmed this estimate experimentally by reflection measurements, where we subtracted the reflection of

the QDPD stack from that of the Au/ITO substrate, which yielded a comparable absorbance at 1330 nm of 27.7% (see Supporting Information S8). Interestingly, this absorption is nearly identical to the EQE of the QDPDs, which highlights the near-unity charge-carrier extraction—estimated for the given EQE at 97%—from the photoactive layer. As shown in Figure 3c, the extraction efficiency is closely related to the active layer thickness, reducing from 97% for a 50 nm-thick n-PbS layer to 79% for a 400 nm-thick layer. Probably, the longer transport time for charge carriers in thicker QD films enhances the charge carrier loss through trapping and recombination.

Figure 4 summarizes the results of a bending durability analysis of QDPDs with an ultrathin, 50 nm n-PbS absorber layer and similar devices with 200 and 400 nm thick n-PbS layers for comparison. We will refer to these devices as QDPD-50, QDPD-200, and QDPD-400, respectively. In the first experiment, we measured the dark and photocurrent of a QDPD-50 after different bending cycles under a 7-mm bending radius. As shown in Figure 4a, the J - V curves of such a QDPD remained unchanged after 10^5 bending cycles. Obviously, this result leads to a constant dark and photocurrent measured at -1 V, which concurs with QDPD-50 featuring a constant EQE throughout the bending cycles (see Figure 4b,c). This result contrasts starkly with those of QDPD-200 and QDPD-400, for which the EQE drops to 81 and 69% after 10^5 bending cycles, respectively. It thus appears that

QDPDs with a thinner active layer better withstand degradation due to repetitive bending, for which a constant EQE during 10^5 cycles sets a new benchmark in flexible colloidal QD optoelectronics.

To further understand the origin of the performance loss in the case of QDPD-200 and QDPD-400, we analyzed the device surfaces after bending using SEM. As can be seen in Figure 4d–f, cracks emerge after repetitive bending in QDPD-200 and QDPD-400, but not in QDPD-50. In Supporting Information S9, we show cross-section SEM images (Supporting Information S9) of the QDPDs with thin (50 nm) and thick (400 nm) active layer devices taken near the edges of a crack, which indicate that cracking comes with delamination in the thick device. Given the stark difference between the thickness of the PET substrate (0.18 mm) and the QDPD stacks—regardless of the n-PbS film thickness, this difference in bending stability is probably not related to a different strain induced in the QD film upon bending. Moreover, computational studies indicate that densely packed QD films with short inorganic ligands may withstand a strain of more than 10% before yielding,⁴² which is well below the strain attained in the bending cycles used here. Therefore, the bending-induced damage in thicker films could reflect the thickness-dependent mechanical properties of QD films. Such a link between thickness-dependent mechanical properties and differences in microstructure has been made for Cu films.³⁴ Interestingly, depending on the film thickness, deposited nanoparticle films are expected to crack upon drying, with critical thicknesses in the range of 50 nm.⁴³ As a result, QD films that are a few tens of nanometers in thickness may have better elastic properties and withstand higher strain before fracture.

In Figure 4g,h, we display the results of additional tests on QDPD-50, where we changed the bending angle from 0 to 180° in steps of 30°. As can be seen, additional bending has no impact on the overall J – V curves or on the EQE until a 120° bending angle (Supporting Information S10). Figure 4i and Supporting Information S11 compare the preserved EQE vs bending cycles obtained here on QDPD-50 with literature reports on flexible optoelectronic QD devices.^{22,32,37,44–46} As can be seen, retaining almost 100% of the initial EQE after 100,000 bending cycles—brought about by reducing the thickness of the photoactive layer and thus minimizing strain—is a unique result that sets a new reference for flexible QD optoelectronics.

CONCLUSION

In summary, we demonstrate flexible colloidal QD photodetectors that withstand at least 100,000 bending cycles while featuring a near-unity carrier extraction efficiency of 97%. These characteristics are obtained by implementing a QD design based on an ultrathin absorber layer. The resulting photodiodes attain a +1/–1 V rectification ratio of 1700 and exhibit an EQE of 27%. This high EQE results from the formation of a Fabry–Pérot cavity within the QDPDs, which enhances light absorption by 3.4-fold. Moreover, by reducing the size of the contact pads to inhibit capacitance effects, these ultrathin, flexible QDPDs exhibit response times as short as 20 ns. We suggest that the exceptional bending stability of these QDPDs reflects the better mechanical properties of thin versus thick QD films, possibly because thick films are more prone to cracking upon drying. Further improving the bending performance of the device in the application, introducing an additional layer, such as encapsulation, could potentially reduce the strain

experienced by the QD layers, possibly improving their stretchability and durability. This work expands the potential applications of flexible colloidal QD optoelectronic devices in the fields of displays, wearable sensors, on-skin electronics, robotics, and so on.

METHODS

Colloidal QD Synthesis. PbS quantum dots absorbing at 950 and 1330 nm were synthesized using lead oleate and N,N' -disubstituted thioureas as precursors.⁴⁷ Details on the QD synthesis and an overview of QD characteristics can be found in Supporting Information S1.

Preparation of ZnO Film. ZnO nanocrystals (NCs) were synthesized following a standard method as described in the article.⁴⁸ ZnO NCs were dispersed in a solution of 2% butylamine in chloroform at a concentration of 40 mg mL⁻¹. The ZnO NCs solution was filtered through a filter (0.45 μm) and stored in the refrigerator for future use.

Fabrication of the Flexible QD Photodiode. Before fabrication, the PET/ITO substrates were ultrasonically cleaned with acetone, ethanol, and deionized water; stuck on the glass with a double-sided tape; and then treated with O₂ plasma. ZnO NCs in chloroform (40 mg mL⁻¹) were spun on top of the substrate with a spin speed of 2500 rpm for 1 min, annealed at 80° for 30 min, and then also treated with O₂ plasma. The PbS QD solution was then deposited on the ZnO layer via the layer-by-layer method: for each layer, 40 μL of the QD solution was dropped and spun at 2500 rpm for 30 s. Oleate-capped QDs are electrically insulating, and the ligands must be replaced by shorter ligands. For the PbS-TBAI layer, TBAI solution (10 mg mL⁻¹ in methanol) was applied to the substrate for 30 s and spun at 2500 rpm for 10 s, followed by two-time acetonitrile rinsing. For the optimized concentration gradient ligand exchange method for the EDT-exchanged PbS layer, the first layer was used with 25 mg/mL QDs and EDT solution (0.005 vol % in acetonitrile), the second layer was used with 25 mg/mL QDs and EDT solution (0.01 vol % in acetonitrile), and the third layer was used with 50 mg/mL QDs and EDT solution (0.02 vol % in acetonitrile). Finally, Au (80 nm) was thermally evaporated on the PbS film, and then the device was stripped from the glass.

Device Characterizations. J – V measurements were taken using a sourcemeter (Keithley 2400) under a N₂ atmosphere. The temporal response of each photodetector was evaluated by measuring the transient photocurrent (TPC) recorded with a 1-GHz oscilloscope (DSO8104A Infinium, Agilent), while a 150 fs pulsed laser (PHAROS, Light Conversion) with a 200-kHz repetition rate illuminated each individual photodetector pixel. All reported TPC experiments were done using 1030 nm excitation without external bias across the device. The I – V curve, detectivity, EQE, and carrier extraction efficiency were measured at 1.5 mm diameter devices. The noise spectrum is measured by the preamplifier and oscilloscope. The signal has been amplified by 10⁸ V/A by a preamplifier and is measured by the oscilloscope under FFT mode. UPS measurements were conducted by using a Physical Electronics PHI 5000 Versa Probe instrument with a monochromatic 21.2 eV (He I) photon beam. XRF was measured using a Rigaku CG Energy Dispersive X-ray Fluorescence specimen. Scanning electron microscopy (SEM) images were obtained with a Hitachi S-5200 microscope. The optical absorption measurements under reflection mode were performed with a PerkinElmer Lambda 950 UV–vis–NIR spectrophotometer (Supporting Information S12). Bending durability and bending angles were measured using a homemade measurement system (Supporting Information S13 and S14). The optical and electrical field distributions in the photodetector simulation using the transfer matrix method (Lumerical STACK optical solver) and the parameter settings for the simulation of the QDPDs are listed in Supporting Information S15.

■ ASSOCIATED CONTENT

SI Supporting Information

The Supporting Information is available free of charge at <https://pubs.acs.org/doi/10.1021/acsami.4c21940>.

Additional detailed experimental data, including the syntheses and preparation details of QDs and photodetectors; calculation and simulation of detectivity, response time, and electrical field distribution; cross-section SEM images and absorption measurement; measurement parameters and setup of bending (PDF)

■ AUTHOR INFORMATION

Corresponding Authors

Yu-Hao Deng – Physics and Chemistry of Nanostructures Group, Ghent University, Gent 9000, Belgium; Center for Nano and Biophotonics, Ghent University, Gent 9052, Belgium; Email: yuhao.deng@ugent.be

Zeger Hens – Physics and Chemistry of Nanostructures Group, Ghent University, Gent 9000, Belgium; Center for Nano and Biophotonics, Ghent University, Gent 9052, Belgium; orcid.org/0000-0002-7041-3375; Email: zegeer.hens@ugent.be

Authors

Ezat Kheradmand – Physics and Chemistry of Nanostructures Group, Ghent University, Gent 9000, Belgium; Center for Nano and Biophotonics, Ghent University, Gent 9052, Belgium

Chao Pang – Center for Nano and Biophotonics and Photonics Research Group, Ghent University, Gent 9052, Belgium

Abu Bakar Siddik – Imec, Leuven 3001, Belgium; Department of Electrical Engineering (ESAT), KU Leuven, Leuven 3001, Belgium; orcid.org/0000-0001-5133-7664

Jing Bai – Physics and Chemistry of Nanostructures Group, Ghent University, Gent 9000, Belgium; Center for Nano and Biophotonics, Ghent University, Gent 9052, Belgium; orcid.org/0000-0002-3361-0433

Itai Lieberman – Imec, Leuven 3001, Belgium

Pieter Geiregat – Physics and Chemistry of Nanostructures Group, Ghent University, Gent 9000, Belgium; Center for Nano and Biophotonics, Ghent University, Gent 9052, Belgium; Core Facility for Non-linear Microscopy and Spectroscopy, Gent 9000, Belgium; orcid.org/0000-0001-7217-8738

Dries Van Thourhout – Center for Nano and Biophotonics and Photonics Research Group, Ghent University, Gent 9052, Belgium; orcid.org/0000-0003-0111-431X

Complete contact information is available at: <https://pubs.acs.org/doi/10.1021/acsami.4c21940>

Notes

The authors declare no competing financial interest.

■ ACKNOWLEDGMENTS

Z.H., D.V.T., and P.G. acknowledge FWO-Vlaanderen for research funding (FWO projects G0B2921N and G0C5723N). Z.H. acknowledges Ghent University (BOF-GOA24021) for funding. Y.D. acknowledges Ghent University for a postdoctoral research fellowship (BOF23/DOC/027). The work also received funding from the European Research Council (ERC)

under the innovation program grant agreement no. 884963 (ERC AdG NARIOS).

■ REFERENCES

- (1) Xie, C.; Yan, F. Flexible photodetectors based on novel functional materials. *Small* **2017**, *13* (43), 1701822.
- (2) Choi, M. K.; Yang, J.; Hyeon, T.; Kim, D.-H. Flexible quantum dot light-emitting diodes for next-generation displays. *Npj Flexible Electron.* **2018**, *2* (1), 10.
- (3) Kagan, C. R. Flexible colloidal nanocrystal electronics. *Chem. Soc. Rev.* **2019**, *48* (6), 1626–1641.
- (4) Kim, J.-Y.; Yun, Y. J.; Jeong, J.; Kim, C.-Y.; Müller, K.-R.; Lee, S.-W. Leaf-inspired homeostatic cellulose biosensors. *Sci. Adv.* **2021**, *7* (16), No. eabe7432.
- (5) Zheng, S.; Li, W.; Ren, Y.; Liu, Z.; Zou, X.; Hu, Y.; Guo, J.; Sun, Z.; Yan, F. Moisture-wicking, breathable, and intrinsically antibacterial electronic skin based on dual-gradient poly (ionic liquid) nanofiber membranes. *Adv. Mater.* **2022**, *34* (4), 2106570.
- (6) Li, Y.; Xu, G.; Cui, C.; Li, Y. Flexible and semitransparent organic solar cells. *Adv. Energy Mater.* **2018**, *8* (7), 1701791.
- (7) Song, W.; Yu, K.; Zhou, E.; Xie, L.; Hong, L.; Ge, J.; Zhang, J.; Zhang, X.; Peng, R.; Ge, Z. Crumple durable ultraflexible organic solar cells with an excellent power-per-weight performance. *Adv. Funct. Mater.* **2021**, *31* (30), 2102694.
- (8) Zhang, C.; Yin, X.; Qian, G.; Chen, G.; Iqbal, S.; Que, W. Paper-Based Lead Sulfide Quantum Dot Heterojunction Photodetectors. *Adv. Mater. Technol.* **2024**, *9* (3), 2301723.
- (9) *Colloidal quantum dot optoelectronics and photovoltaics*; Konstantatos, G. Cambridge University Press, 2013.
- (10) Kovalenko, M. V.; Manna, L.; Cabot, A.; Hens, Z.; Talapin, D. V.; Kagan, C. R.; Klimov, V. I.; Rogach, A. L.; Reiss, P.; Milliron, D. J.; et al. Prospects of nanoscience with nanocrystals. *ACS Nano* **2015**, *9* (2), 1012–1057.
- (11) Kagan, C. R.; Lifshitz, E.; Sargent, E. H.; Talapin, D. V. Building devices from colloidal quantum dots. *Science* **2016**, *353* (6302), aac5523.
- (12) García de Arquer, F. P.; Talapin, D. V.; Klimov, V. I.; Arakawa, Y.; Bayer, M.; Sargent, E. H. Semiconductor quantum dots: Technological progress and future challenges. *Science* **2021**, *373* (6555), No. eaaz8541.
- (13) Deng, Y.-H.; Pang, C.; Kheradmand, E.; Leemans, J.; Bai, J.; Minjauw, M.; Liu, J.; Molkens, K.; Beeckman, J.; Detavernier, C.; et al. Short-Wave Infrared Colloidal QDs Photodetector with Nanosecond Response Times Enabled by Ultrathin Absorber Layers. *Adv. Mater.* **2024**, *36* (28), 2402002.
- (14) Li, M.; Bao, Y.; Hui, W.; Sun, K.; Gu, L.; Kang, X.; Wang, D.; Wang, B.; Deng, H.; Guo, R.; et al. In Situ Surface Reconstruction toward Planar Heterojunction for Efficient and Stable FAPbI₃ Quantum Dot Solar Cells. *Adv. Mater.* **2024**, *36* (6), 2309890.
- (15) Bao, Y.; Li, M.; Jin, H.; Wang, X.; Zeng, J.; Feng, Y.; Hui, W.; Wang, D.; Gu, L.; Zhang, J.; Hua, Y. Directional Charge Carrier Management Enabled by Orderly Arranged Perovskite Heterodomain with Defined Size for Self-Powered Photodetectors. *Adv. Funct. Mater.* **2024**, *34* (44), 2404697.
- (16) Saleh, R.; Barth, M.; Eberhardt, W.; Zimmermann, A. Bending setups for reliability investigation of flexible electronics. *Micromachines* **2021**, *12* (1), 78.
- (17) Kim, T.-W.; Lee, J.-S.; Kim, Y.-C.; Joo, Y.-C.; Kim, B.-J. Bending strain and bending fatigue lifetime of flexible metal electrodes on polymer substrates. *Materials* **2019**, *12* (15), 2490.
- (18) Harris, K.; Elias, A.; Chung, H.-J. Flexible electronics under strain: a review of mechanical characterization and durability enhancement strategies. *J. Mater. Sci.* **2016**, *51*, 2771–2805.
- (19) Chen, Z.; Cotterell, B.; Wang, W.; Guenther, E.; Chua, S.-J. A mechanical assessment of flexible optoelectronic devices. *Thin Solid Films* **2001**, *394* (1–2), 201–205.
- (20) Zhao, Z.; Fu, H.; Tang, R.; Zhang, B.; Chen, Y.; Jiang, J. Failure mechanisms in flexible electronics. *Int. J. Smart Nano Mater.* **2023**, *14* (4), 510–565.

- (21) Jain, S.; Willander, M.; Maes, H. Stresses and strains in epilayers, stripes and quantum structures of III-V compound semiconductors. *Semicond. Sci. Technol.* **1996**, *11* (5), 641.
- (22) Xu, Z.; Han, Y.; Bai, Y.; Chen, X.; Guo, J.; Zhang, L.; Gong, C.; Luo, Q.; Zhang, T.; Ma, C.-Q. Thermoplastic elastomer enhanced interface adhesion and bending durability for flexible organic solar cells. *Npj Flexible Electron.* **2022**, *6* (1), 56.
- (23) Liang, X.; Liu, Y.; Liu, P.; Yang, J.; Liu, J.; Yang, Y.; Wang, B.; Hu, J.; Zhang, L.; Yang, G.; et al. Large-area flexible colloidal-quantum-dot infrared photodiodes for photoplethysmogram signal measurements. *Sci. Bull.* **2023**, *68* (7), 698–705.
- (24) Seo, J. H.; Hwang, I.; Um, H.-D.; Lee, S.; Lee, K.; Park, J.; Shin, H.; Kwon, T.-H.; Kang, S. J.; Seo, K. Cold isostatic-pressured silver nanowire electrodes for flexible organic solar cells via room-temperature processes. *Adv. Mater.* **2017**, *29* (30), 1701479.
- (25) Sun, Y.; Chang, M.; Meng, L.; Wan, X.; Gao, H.; Zhang, Y.; Zhao, K.; Sun, Z.; Li, C.; Liu, S.; Wang, H. Flexible organic photovoltaics based on water-processed silver nanowire electrodes. *Nat. Electron.* **2019**, *2* (11), 513–520.
- (26) Qin, F.; Wang, W.; Sun, L.; Jiang, X.; Hu, L.; Xiong, S.; Liu, T.; Dong, X.; Li, J.; Jiang, Y.; et al. Robust metal ion-chelated polymer interfacial layer for ultraflexible non-fullerene organic solar cells. *Nat. Commun.* **2020**, *11* (1), 4508.
- (27) Chen, X.; Xu, G.; Zeng, G.; Gu, H.; Chen, H.; Xu, H.; Yao, H.; Li, Y.; Hou, J.; Li, Y. Realizing ultrahigh mechanical flexibility and >15% efficiency of flexible organic solar cells via a “welding” flexible transparent electrode. *Adv. Mater.* **2020**, *32* (14), 1908478.
- (28) Qin, F.; Sun, L.; Chen, H.; Liu, Y.; Lu, X.; Wang, W.; Liu, T.; Dong, X.; Jiang, P.; Jiang, Y.; Wang, L. 54 cm² Large-Area Flexible Organic Solar Modules with Efficiency Above 13%. *Adv. Mater.* **2021**, *33* (39), 2103017.
- (29) Han, J.; Bao, F.; Huang, D.; Wang, X.; Yang, C.; Yang, R.; Jian, X.; Wang, J.; Bao, X.; Chu, J. A universal method to enhance flexibility and stability of organic solar cells by constructing insulating matrices in active layers. *Adv. Funct. Mater.* **2020**, *30* (38), 2003654.
- (30) Peng, Z.; Xian, K.; Cui, Y.; Qi, Q.; Liu, J.; Xu, Y.; Chai, Y.; Yang, C.; Hou, J.; Geng, Y.; Ye, L. Thermoplastic elastomer tunes phase structure and promotes stretchability of high-efficiency organic solar cells. *Adv. Mater.* **2021**, *33* (49), 2106732.
- (31) Sheikh, T.; Mir, W. J.; Alofi, A.; Skoroterski, M.; Zhou, R.; Nematulloev, S.; Hedhili, M. N.; Hassine, M. B.; Khan, M. S.; Yorov, K. E.; Hasanov, B. E. Surface-Reconstructed InAs Colloidal Nanorod Quantum Dots for Efficient Deep-Shortwave Infrared Emission and Photodetection. *J. Am. Chem. Soc.* **2024**, *146* (42), 29094–29103.
- (32) Kim, C.; Kozakci, I.; Lee, S. Y.; Kim, B.; Kim, J.; Lee, J.; Ma, B. S.; Oh, E. S.; Kim, T. S.; Lee, J. Y. Quantum Dot-Siloxane Anchoring on Colloidal Quantum Dot Film for Flexible Photovoltaic Cell. *Small* **2023**, *19* (41), 2302195.
- (33) Sun, X.; Wang, C.; Zhang, J.; Liu, G.; Zhang, G.; Ding, X.; Zhang, G.; Sun, J. Thickness dependent fatigue life at microcrack nucleation for metal thin films on flexible substrates. *J. Phys. D: Appl. Phys.* **2008**, *41* (19), 195404.
- (34) Kim, B.-J.; Shin, H.-A.-S.; Lee, J.-H.; Yang, T.; Haas, T.; Gruber, P.; Choi, I.-S.; Kraft, O.; Joo, Y.-C. Effect of film thickness on the stretchability and fatigue resistance of Cu films on polymer substrates. *J. Mater. Res.* **2014**, *29* (23), 2827–2834.
- (35) Jing, H.; Peng, R.; Ma, R.-M.; He, J.; Zhou, Y.; Yang, Z.; Li, C.-Y.; Liu, Y.; Guo, X.; Zhu, Y.; et al. Flexible ultrathin single-crystalline perovskite photodetector. *Nano Lett.* **2020**, *20* (10), 7144–7151.
- (36) Chuang, C.-H. M.; Brown, P. R.; Bulović, V.; Bawendi, M. G. Improved performance and stability in quantum dot solar cells through band alignment engineering. *Nat. Mater.* **2014**, *13* (8), 796–801.
- (37) Xu, W.; Chen, B.; Zhang, Z.; Liu, Y.; Xian, Y.; Wang, X.; Shi, Z.; Gu, H.; Fei, C.; Li, N.; et al. Multifunctional entinostat enhances the mechanical robustness and efficiency of flexible perovskite solar cells and minimodules. *Nat. Photonics* **2024**, *18*, 379–387.
- (38) Peng, M.; Wen, Z.; Sun, X. Recent Progress of Flexible Photodetectors Based on Low-Dimensional II–VI Semiconductors and Their Application in Wearable Electronics. *Adv. Funct. Mater.* **2023**, *33* (11), 2211548.
- (39) Xu, Q.; Meng, L.; Sinha, K.; Chowdhury, F. I.; Hu, J.; Wang, X. Ultrafast colloidal quantum dot infrared photodiode. *ACS Photonics* **2020**, *7* (5), 1297–1303.
- (40) Wang, B.-X.; Qin, X.; Duan, G.; Yang, G.; Huang, W.-Q.; Huang, Z. Dielectric-Based Metamaterials for Near-Perfect Light Absorption. *Adv. Funct. Mater.* **2024**, *34* (37), 2402068.
- (41) Pala, R. A.; White, J.; Barnard, E.; Liu, J.; Brongersma, M. L. Design of plasmonic thin-film solar cells with broadband absorption enhancements. *Adv. Mater.* **2009**, *21* (34), 3504–3509.
- (42) Wang, Z.; Srinivasan, S.; Dai, R.; Rana, A.; Nian, Q.; Solanki, K.; Wang, R. Y. Inorganically Connecting Colloidal Nanocrystals Significantly Improves Mechanical Properties. *Nano Lett.* **2023**, *23* (11), 4916–4922.
- (43) Singh, K. B.; Tirumkudulu, M. S. Cracking in drying colloidal films. *Phys. Rev. Lett.* **2007**, *98* (21), 218302.
- (44) Jiang, W.; Lee, S.; Zhao, K.; Lee, K.; Han, H.; Oh, J.; Lee, H.; Kim, H.; Koo, C. M.; Park, C. Flexible and Transparent Electrode of Hybrid Ti3C2TX MXene–Silver Nanowires for High-Performance Quantum Dot Light-Emitting Diodes. *ACS Nano* **2022**, *16* (6), 9203–9213.
- (45) Li, X.; Yu, D.; Chen, J.; Wang, Y.; Cao, F.; Wei, Y.; Wu, Y.; Wang, L.; Zhu, Y.; Sun, Z.; et al. Constructing fast carrier tracks into flexible perovskite photodetectors to greatly improve responsivity. *ACS Nano* **2017**, *11* (2), 2015–2023.
- (46) Kim, Y.; Kim, J.; Kim, H.-M.; Jang, J. Quantum-Dots Photosensor with Wide Bandgap P-Type and N-Type Oxide Semiconductors for High Detectivity and Responsivity. *Adv. Mater. Technol.* **2020**, *5* (1), 1900857.
- (47) Hendricks, M. P.; Campos, M. P.; Cleveland, G. T.; Jen-La Plante, I.; Owen, J. S. A tunable library of substituted thiourea precursors to metal sulfide nanocrystals. *Science* **2015**, *348* (6240), 1226–1230.
- (48) Beek, W. J.; Wienk, M. M.; Kemerink, M.; Yang, X.; Janssen, R. A. Hybrid zinc oxide conjugated polymer bulk heterojunction solar cells. *J. Phys. Chem. B* **2005**, *109* (19), 9505–9516.